Supporting Information

Multiscale analysis of large twist ferroelectricity and swirling dislocations in bilayer hexagonal boron nitride

Md Tusher Ahmed,[†,¶] Chenhaoyue Wang,[‡,¶] Amartya S. Banerjee,[‡] and Nikhil Chandra Admal[*,†]

†*Department of Mechanical Science and Engineering, University of Illinois Urbana-Champaign, Urbana, IL, USA*

‡*Department of Materials Science and Engineering, University of California, Los Angeles., Los Angeles, CA, USA*

¶*These authors contributed equally to this work.*

E-mail: admal@illinois.edu

S-1 The continuum substrate

We model the van der Waals (vdW) interaction between a hBN bilayer and a substrate using the Lennard-Jones (LJ) potential in the atomistic simulations. The LJ potential between two atoms at a distance d is given by

$$\psi(d) = 4\epsilon\left[\left(\frac{\sigma}{d}\right)^{12} - \left(\frac{\sigma}{d}\right)^{6}\right], \tag{S-1}$$

where ϵ and σ are the energy and distance parameters, respectively. We approximate the substrate as a homogeneous continuum with a given number density, thereby skipping the explicit modeling of discrete atoms in the substrate, which significantly increases computational cost while providing no additional information. In this study, we chose graphite to be the substrate. The interaction energy between the B and N atoms and the continuum substrate is described by an effective potential U_{sub}[1]:

$$U_{\text{sub}}(\rho_{\text{sub}}, \sigma, \epsilon, z_0) = \frac{4}{3}\pi\rho_{\text{sub}}\epsilon\sigma^3\left[\frac{1}{15}\left(\frac{\sigma}{z_0}\right)^9 - \frac{1}{2}\left(\frac{\sigma}{z_0}\right)^3\right], \tag{S-2}$$

where ρ_{sub} is the number density of the substrate per unit volume, and z_0 is the vertical distance between B and N atoms with the corresponding substrate atoms. The force acting on an hBN basis atom (B or N) in the z-direction, f_{sub}, is computed as

$$f_{\text{sub}}(\rho_{\text{sub}}, \sigma, \epsilon, z_0) = -\frac{4}{3}\pi\rho_{\text{sub}}\epsilon\sigma^2\left[\frac{3}{5}\left(\frac{\sigma}{z_0}\right)^{10} - \frac{3}{2}\left(\frac{\sigma}{z_0}\right)^4\right]. \tag{S-3}$$

The LJ parameters for the interaction between carbon atoms and the basis atoms follows: $\epsilon_{\text{C-B}} = 3.24$ meV and $\sigma_{\text{C-B}} = 0.34$ nm for carbon-boron interaction, $\epsilon_{\text{C-N}} = 4.07$ meV and $\sigma_{\text{C-N}} = 0.34$ nm for carbon-nitrogen interaction[2,3]. The number densities of C (ρ_{C}) is 0.2385 atoms/Å^3. Because the basis atoms contain two different atoms (i.e., B and N), the LJ energy applied on the basis atoms above the substrate is given by

$$U_{\text{sub}}(z_0) = U_{\text{sub}}(\rho_{\text{B}}, \sigma_{\text{C-B}}, \epsilon_{\text{C-B}}, z_0) + U_{\text{sub}}(\rho_{\text{N}}, \sigma_{\text{C-N}}, \epsilon_{\text{C-N}}, z_0). \tag{S-4}$$

The corresponding force is

$$f_{\text{sub}}(z_0) = f_{\text{sub}}(\rho_{\text{B}}, \sigma_{\text{C-B}}, \epsilon_{\text{C-B}}, z_0) + f_{\text{sub}}(\rho_{\text{N}}, \sigma_{\text{C-N}}, \epsilon_{\text{C-N}}, z_0). \tag{S-5}$$

S-2 Details of the numerical implementation

In this study, the BFIM model is implemented under periodic boundary conditions (PBC) to facilitate direct comparison between atomic-scale results from LAMMPS and those obtained from the BFIM framework. The use of PBC enables the application of the fast Fourier transform (FFT) for efficient evaluation of spatial gradients. Accordingly, we employ the pseudospectral method[4] to solve the governing equation in Eqn [15] where the spatial gradients are computed via FFT. The solution is advanced in time using an explicit Runge–Kutta (RK) scheme with a fixed time step δt, yielding the following discretized equations:

$$\boldsymbol{\phi}_\alpha^{n+1} = \boldsymbol{\phi}_\alpha^n + \frac{1}{6m}\left(\boldsymbol{k}_{\alpha 1} + 2\boldsymbol{k}_{\alpha 2} + 2\boldsymbol{k}_{\alpha 3} + \boldsymbol{k}_{\alpha 4}\right), \text{ where}$$

$$\boldsymbol{k}_{\alpha 1} = \delta t \boldsymbol{f}_\alpha|_{\boldsymbol{\phi}=\boldsymbol{\phi}^n}, \quad \boldsymbol{k}_{\alpha 2} = \delta t \boldsymbol{f}_\alpha|_{\boldsymbol{\phi}=\boldsymbol{\phi}^n+\frac{\boldsymbol{k}_{\alpha 1}}{2}}, \quad \boldsymbol{k}_{\alpha 3} = \delta t \boldsymbol{f}_\alpha|_{\boldsymbol{\phi}=\boldsymbol{\phi}^n+\frac{\boldsymbol{k}_{\alpha 2}}{2}}, \quad \boldsymbol{k}_{\alpha 4} = \delta t \boldsymbol{f}_\alpha|_{\boldsymbol{\phi}=\boldsymbol{\phi}^n+\boldsymbol{k}_{\alpha 3}}.$$

Here, $\phi_\alpha^n := \phi_\alpha(\cdot, t_n)$, $\boldsymbol{f}_\alpha$ represents the right-hand-side of Eqn [15], and $\boldsymbol{f}_\alpha|_{\boldsymbol{\phi}=\boldsymbol{\phi}^n}$ denotes the evaluation of $\boldsymbol{f}_\alpha$ using $\boldsymbol{\phi}_\alpha^n$. The spatial derivatives in $\boldsymbol{f}_\alpha$ are computed using FFT. Here, we consider $m = 1$. The simulation domain was discretized using a 64×64 grid, which ensures that the width of the interface dislocations is reasonably resolved. The temporal discretization varies according to the simulation domain size, ensuring the numerical scheme remains stable. Similar to the atomistic simulations, the system is first allowed to equilibrate in the absence of an electric field, resulting in the formation of interface dislocations. Subsequently, the out-of-plane electric field is applied.

In zero-electric-field relaxation simulations, we generally consider a trivial initial condition, with all the displacement components in both layers being zero. However, for equi-biaxially stretched bilayer hBN, the method requires a physics-informed initial condition, as

presented below

$$\boldsymbol{\phi}_{\mathrm{t}} - \boldsymbol{X}_{\mathrm{t}} = u_a \left[\sin\left(\frac{2\pi\zeta^1}{l_m}\right) \hat{\boldsymbol{l}}^2 + \sin\left(\frac{2\pi\zeta^2}{l_m}\right) \hat{\boldsymbol{l}}^1 \right], \tag{S-6a}$$

$$\boldsymbol{\phi}_{\mathrm{b}} - \boldsymbol{X}_{\mathrm{b}} = -(\boldsymbol{\phi}_{\mathrm{t}} - \boldsymbol{X}_{\mathrm{t}}). \tag{S-6b}$$

Here, $\boldsymbol{\phi}_{\mathrm{t}} - \boldsymbol{X}_{\mathrm{t}}$ and $\boldsymbol{\phi}_{\mathrm{b}} - \boldsymbol{X}_{\mathrm{b}}$ refer to the displacement perturbation provided to the top and bottom layers, respectively. $u_a = 0.25$Å is considered as the amplitude of the displacement perturbation. $\boldsymbol{\zeta}_1$ and $\boldsymbol{\zeta}_2$ refer to the non-orthogonal basis of the simulation domain where $\boldsymbol{\zeta}_1$ corresponds to the X_1 in Figure 3 of the main paper while, $\boldsymbol{\zeta}_2$ is aligned with the other arm of the parallelogram. l_m is the length of the moiré superlattice. Finally, $\hat{\boldsymbol{l}}^i = \hat{\boldsymbol{n}} \times \hat{\boldsymbol{\zeta}}^i$ is the reciprocal basis vectors to $\hat{\boldsymbol{\zeta}}^i$ where, $\hat{\boldsymbol{n}}$ is the out-of-plane normal unit vector.

S-3 Computational details of density functional theory calculations of the GSFE and PL

Density functional theory (DFT) calculations, as implemented within the ABINIT package[5,6] were used for computing stacking fault energy and out-of-plane polarization values for bilayer hBN. Polarization calculations were carried out based on the Berry phase approach.[7] The exchange-correlation functional was treated using the Perdew-Burke-Ernzerhof (PBE) formulation of the generalized gradient approximation (GGA).[8] Projector augmented-wave (PAW) pseudopotentials[9] were used for boron and nitrogen atoms. A plane-wave cutoff energy of 70 Ha was set to ensure accurate convergence. For ground-state energy calculations, a Monkhorst–Pack k-point mesh[10] of $9 \times 9 \times 1$ grid points was used, while a finer mesh of $15 \times 15 \times 1$ k-points was employed for polarization calculations. To account for van der Waals interactions between the two layers, the vdW-DFT-D3(BJ) correction was applied.[11] A vacuum spacing of 20 Åwas introduced to ensure the bilayer hBN remained isolated and to avoid interactions between periodic images that could affect polarization

values. Additionally, appropriate Coulomb corrections consistent with the system geometry[12,13] were applied. The convergence criteria were set to 1×10^{-12} for self-consistent field (SCF) calculations of small twist hBN and 1×10^{-9} for the large twist case, and 1×10^{-9} for wavefunction optimization. A 21×21 displacement grid (corresponding to a fractional step size of 1/20 between adjacent stacking configurations) was used in all calculations to produce precise energy and polarization landscapes. Both the GGA-PBE functional with vdW-DFT-D3(BJ) correction and a meta-GGA functional[14] were utilized to compute the GSFE and polarization patterns for large-twist hBN, and yielded consistent results across both functionals.

S-4 In-plane polarization density map of AA-stacked bilayer hexagonal boron nitride

Fig. 1 shows the in-plane polarization density map of AA-stacked bilayer hBN computed using DFT. The interplanar spacing is maintained at 3.33 Å, similar to the out-of-plane polarization density calculations.

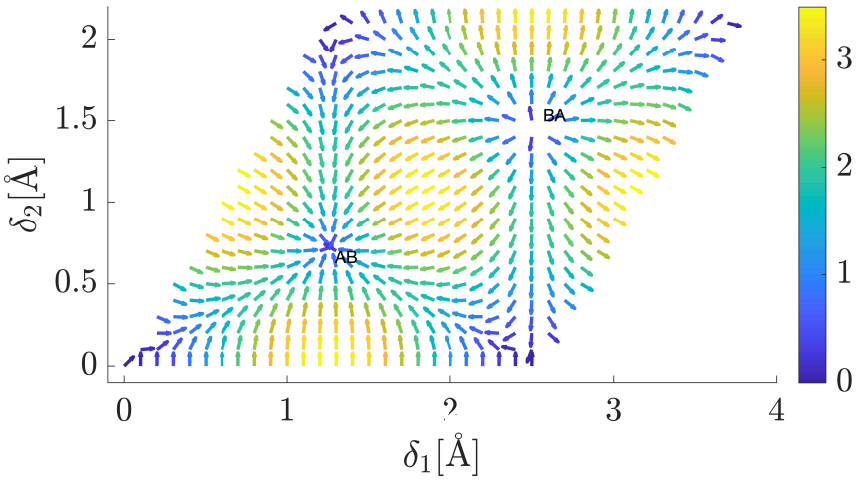

Figure 1: In-plane polarization $[mC/m^2]$ vector field, computed using DFT, plotted as a function of the relative displacement between the two layers of an AA-stacked bilayer hBN.

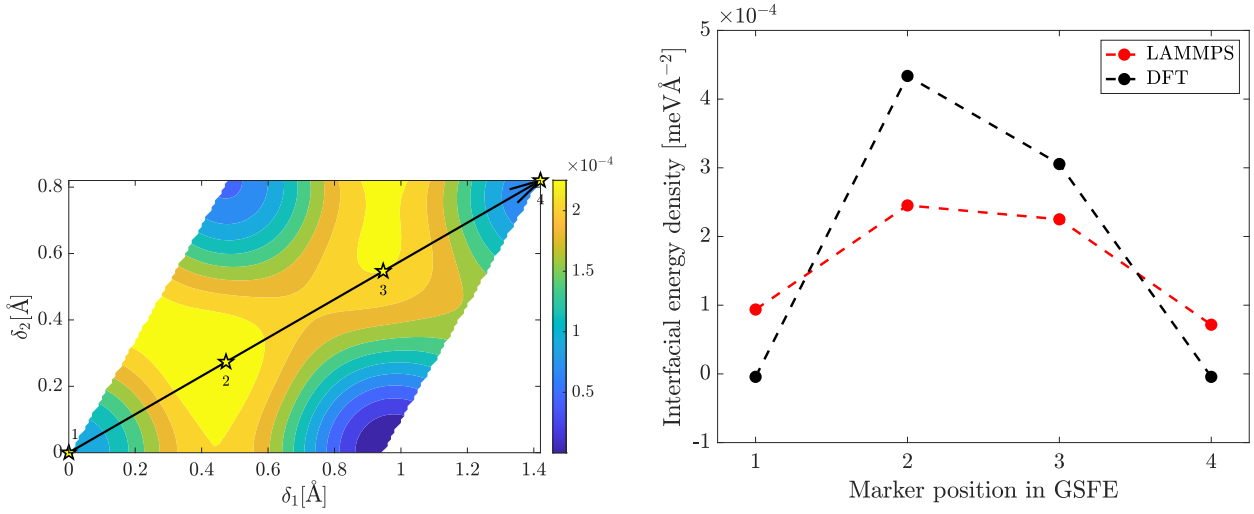

(a) (b)

Figure 2: (a) Generalized stacking fault energy (GSFE) map $[meV\text{Å}^{-2}]$ plot of 21.786789° twisted bilayer hBN at equilibrium spacing, computed using LAMMPS with markers at different characteristic stacking. (b) compares the interfacial energy density computed using LAMMPS and DFT for the marked stacking.

S-5 GSFE plot for 21.786789° twisted bilayer hBN at equilibrium spacing

Fig. 2 compares the GSFE of 21.786789° twisted bilayer hBN at equilibrium spacing, computed using DFT and LAMMPS. Fig. 2a shows the LAMMPS-computed GSFE with the characteristic stackings marked. Clearly, the overall trend of the plot in Fig. 2a matches that of the LAMMPS-computed GSFE under a 28% compression, shown in Figure 10 of the main paper. However, the maximum energy density is 10^{-2} times lower than that under 28% compression. Fig. 2b compares the interfacial energy density of the marked stacking shown in Fig. 2a, computed using DFT and LAMMPS. The DFT-predicted interfacial energy densities are slightly higher than the LAMMPS-predicted densities. This clearly illustrates that at equilibrium interlayer spacing, the GSFEs computed using DFT and LAMMPS show comparable magnitudes and trends, indicating that discrepancies emerge primarily under out-of-plane compression.

S-6 Calculation of Peierls stress from the GSFE of a 21.786789° twisted bilayer hexagonal boron nitride

The goal of this section is to investigate the extent to which Peierls stress of interface dislocations may influence spontaneous polarization in a bilayer hBN that is heterodeformed relative to the 21.786789° twist configuration. The Peierls stress is the smallest stress required to move a dislocation in the material.[15] We utilize the methodology provided by Lu[15] to predict the Peierls stress for interface dislocations in heterodeformed bilayer hBN from the GSFE of 28% out-of-plane compressed 21.786789° twisted bilayer hBN. The Peierls stress is computed using

$$\sigma_p = \frac{2\mu_{3D}}{1-\nu} \exp\left(\frac{-4\pi\zeta}{b}\right), \tag{S-7}$$

where ζ and b are the core width and magnitude of the Burgers vector of the interface dislocation. μ_{3D} and ν are the Lamé constants of 2D hBN, taken from Jung et al.[16]. ζ, the core width of the interface dislocation under out-of-plane compression, is computed using the expression

$$\zeta = \frac{\mu_{3D} b}{2\pi \times 4\pi F_{max}}. \tag{S-8}$$

Here, F_{max} is the maximum slope of the energy landscape between two neighboring energy minima. For 28% out-of-plane compressed 21.786789° twisted bilayer hBN, we found $F_{max} = 0.272064 meV\text{Å}^{-3}$. Using this value, the core width, ζ is computed to be 158.11Å. The value of core width is comparable to the core width predicted by Pei et al.[17] for twisted bilayer graphene. Using the core width, ζ, the Peierls stress is found to be negligible, close to zero. This negligible Peierls stress is a consequence of the large core width in bilayer 2D materials, which can instantaneously initiate dislocation motion under applied load.

References

(1) Choi, M.-k.; Sung, S. H.; Hovden, R.; Tadmor, E. B. Elastic plate basis for the deformation and electron diffraction of twisted bilayer graphene on a substrate. *Physical Review B* **2024**, *110*, 024116.

(2) Baowan, D.; Hill, J. M. Nested boron nitride and carbon-boron nitride nanocones. *Micro & Nano Letters* **2007**, *2*, 46–49.

(3) Heinz, H.; Lin, T.-J.; Kishore Mishra, R.; Emami, F. S. Thermodynamically consistent force fields for the assembly of inorganic, organic, and biological nanostructures: the INTERFACE force field. *Langmuir* **2013**, *29*, 1754–1765.

(4) Hussaini, M. Y.; Zang, T. A. Spectral methods in fluid dynamics. *Annual review of fluid mechanics* **1987**, *19*, 339–367.

(5) Gonze, X. et al. ABINIT: First-principles approach to material and nanosystem properties. *Computer Physics Communications* **2009**, *180*, 2582–2615.

(6) Gonze, X.; Amadon, B.; Antonius, G.; Arnardi, F.; Baguet, L.; Beuken, J.-M.; Bieder, J.; Bottin, F.; Bouchet, J.; Bousquet, E.; others The ABINIT project: Impact, environment and recent developments. *Computer Physics Communications* **2020**, *248*, 107042.

(7) King-Smith, R. D.; Vanderbilt, D. Theory of polarization of crystalline solids. *Physical Review B* **1993**, *47*, 1651–1654.

(8) Perdew, J. P.; Burke, K.; Ernzerhof, M. Generalized Gradient Approximation Made Simple. *Physical Review Letters* **1996**, *77*, 3865–3868.

(9) Blöchl, P. E.; Först, C. J.; Schimpl, J. Projector augmented wave method: ab initio molecular dynamics with full wave functions. *Bulletin of Materials Science* **2003**, *26*, 33–41.

(10) Monkhorst, H. J.; Pack, J. D. Special points for Brillouin-zone integrations. *Physical review B* **1976**, *13*, 5188.

(11) Grimme, S.; Antony, J.; Ehrlich, S.; Krieg, H. A consistent and accurate *ab initio* parametrization of density functional dispersion correction (DFT-D) for the 94 elements H-Pu. *The Journal of Chemical Physics* **2010**, *132*, 154104.

(12) Ismail-Beigi, S. Truncation of periodic image interactions for confined systems. *Physical Review B—Condensed Matter and Materials Physics* **2006**, *73*, 233103.

(13) Rozzi, C. A.; Varsano, D.; Marini, A.; Gross, E. K.; Rubio, A. Exact Coulomb cutoff technique for supercell calculations. *Physical Review B—Condensed Matter and Materials Physics* **2006**, *73*, 205119.

(14) Sun, J.; Ruzsinszky, A.; Perdew, J. P. Strongly Constrained and Appropriately Normed Semilocal Density Functional. *Phys. Rev. Lett.* **2015**, *115*, 036402.

(15) Lu, G. *Handbook of Materials Modeling: Methods*; Springer, 2005; pp 793–811.

(16) Jung, J.; DaSilva, A. M.; MacDonald, A. H.; Adam, S. Origin of band gaps in graphene on hexagonal boron nitride. *Nature communications* **2015**, *6*, 6308.

(17) Pei, Z.; Mu, S.; Ming, W. The local strain distribution in bilayer materials: A multiscale study. *Nanoscale* **2020**, *12*, 6456–6461.